JOURNAL OF GUIDANCE, CONTROL, AND DYNAMICS
Vol. 32, No. 3, May–June 2009

Low-Thrust Control of a Lunar Mapping Orbit

Nathan Harl* and Henry J. Pernicka†
Missouri University of Science and Technology, Rolla, Missouri 65409-0050

DOI: 10.2514/1.37098

A method is presented for establishing and maintaining a lunar mapping orbit using continuous-low-thrust propulsion. Optimal control theory is used to maintain a lunar orbit that is low-altitude, near-polar, and sun-synchronous, which are three typical requirements for a successful lunar mapping mission. The analysis of the optimal control problem leads to the commonly seen two-point boundary-value problem, which is solved using a simple indirect shooting algorithm. Simulations are presented for a one-year mapping duration, in which it is shown that an average control force of 0.5 N for a 1000-kg-class spacecraft is required to rotate the orbit plane at the sun-synchronous rate. Because this amounts to a total ΔV of roughly 15 km/s, a fairly large propellant mass of 416 kg would be required from a typical ion thruster for a one-year mission. However, if the science requirements can be fulfilled in a shorter 1–2-month mission, the required propellant mass could be drastically reduced. Also, it is shown that if the desired control accuracy of the sun-synchronous ascending node is relaxed, the required thrust levels can be decreased by roughly 0.2 N.

Introduction

IN 2004, President Bush announced his Vision for Space Exploration (VSE) plan, which defined many goals for NASA to fulfill in the next 20 to 30 years. One of the first and primary goals of the VSE is for NASA to commence unmanned and manned missions to the moon by 2008 and 2020, respectively, with the hope of eventually establishing a manned station or colony on the moon. The main purpose of the unmanned missions will be to facilitate the manned missions by mapping the moon to identify locations of water in the form of ice as possible landing sites. The first unmanned mission under the VSE, the Lunar Reconnaissance Orbiter (LRO), was scheduled to launch in fall 2008 [1]. LRO will consist of a one-year-duration reconnaissance mission using a 50 km polar lunar orbit.

Because the mapping missions will involve using a satellite to continuously image the lunar surface, certain orbital properties for such a satellite will enhance its ability to collect the needed data. First, it is desired for the satellite to be in a low-altitude orbit to provide high imaging resolution. A near-polar orbit is also desired to ensure global coverage of the moon. Finally, it is desired for the satellite to be located in a sun-synchronous orbit, in which the line of nodes rotates at such a rate that the sun will always be in the same orientation with respect to the satellite orbit plane so that imaging will be taken with consistent lighting conditions. Sun-synchronous orbits are also useful in that the thermal environment is identical on a daily basis, which can be beneficial for thermal management of sensitive components needed to perform the mapping mission.

Of the three properties described, the most challenging to achieve is the sun-synchronous condition. This is primarily because lunar sun-synchronous orbits do not exist naturally, unlike sun-synchronous missions about Earth in which the J_2 effect facilitates the generation of sun-synchronous orbits that do not require control maneuvers to rotate the node line. The Earth's equatorial oblateness creates an out-of-plane force that, for orbits with properly specified altitudes and inclinations, rotates an orbit at the sun-synchronous rate. However, because the moon's oblateness is much less than the Earth's, this luxury is not present when attempting to establish a lunar sun-synchronous orbit. Instead, generating and maintaining a lunar sun-synchronous orbit requires continuously applying an out-of-plane thrust to rotate the orbit at the desired rate.

This paper presents a method for establishing a low-altitude, polar, sun-synchronous lunar orbit using continuous low thrust. It is shown that by performing a continuous out-of-plane acceleration, the sun-synchronous condition can be maintained for a long-term mission. Optimal control theory with a Lagrangian performance index is used to determine the required control accelerations. However, as discussed later in the paper, due to the physical inability to control the line of nodes during equatorial crossings, a switch is made between ascending node and inclination control in these regions. This leads to suboptimal (but still effective) trajectories.

The dynamic model used in this study includes the three primary perturbations that a low-altitude lunar orbiter experiences: the perturbations due to the Earth's and sun's gravities and perturbations due to the nonspherical lunar gravity field. The lunar gravity field is modeled using the LP165P gravity model [2] obtained from the NASA Planetary Data System (PDS) Geosciences Node.

Previous Studies

Lunar Mapping Missions

Some of the first lunar mapping missions date back to the 1960s. As the United States and Russia were competing to be the first to perform a manned mission to land on the moon, both countries began conducting unmanned scientific missions to the moon to study the lunar surface and test soft-landing approaches.

NASA began its first set of unmanned lunar missions in the early 1960s with the Ranger program [3]. The goal of each Ranger mission was to take high-resolution images of the moon and return them in real time. Each mission was designed such that the satellite was placed on a collision course with the lunar surface, with pictures of the surface being taken continuously up to impact. However, these missions encountered a number of malfunctions, and only three of the nine missions were successful. Later in the decade, NASA initiated the Lunar Surveyor program [4]. Although the primary goal of this program was to achieve soft landing on the moon, the lunar surveyor satellites also took a large assortment of close-range images of the lunar surface.

Russia also sent an assortment of scientific missions to the moon in the form of the Luna program [5]. Many of these missions involved taking high-resolution images of the lunar surface, and the Luna 3 mission obtained the first images of the far side of the moon. A total

Received 11 February 2008; revision received 30 December 2008; accepted for publication 6 January 2009. Copyright © 2009 by Nathan Harl and Henry J. Pernicka. Published by the American Institute of Aeronautics and Astronautics, Inc., with permission. Copies of this paper may be made for personal or internal use, on condition that the copier pay the $10.00 per-copy fee to the Copyright Clearance Center, Inc., 222 Rosewood Drive, Danvers, MA 01923; include the code 0731-5090/09 $10.00 in correspondence with the CCC.

*Graduate Student, Department of Mechanical and Aerospace Engineering, Toomey Hall, 400 West 13th Street; nrh7b2@mst.edu.

†Associate Professor, Department of Mechanical and Aerospace Engineering, Toomey Hall, 400 West 13th Street; pernicka@mst.edu. Senior Member AIAA.

of 24 missions during the 1960s and 1970s were conducted in the Luna program with fairly substantial scientific gain.

With a renewed interest in the moon in the 1990s, NASA conducted lunar mapping missions that greatly increased knowledge of the moon. Two of these missions were the 1994 Clementine mission [6,7] and the 1998 Lunar Prospector mission [8]. A large amount of the knowledge currently available about the moon, including the lunar gravity model used in this work, comes directly from the results of these two successful missions.

More recently, Park and Junkins [9] proposed possible lunar mapping orbits using a frozen-orbit concept. In such a frozen orbit, the eccentricity, argument of periapsis, and inclination variations are approximately zero. The authors also showed that a near-sun-synchronous orbit exists at an inclination of 101.4 deg, and the line of nodes deviates from the sun-synchronous condition by approximately 10 deg over the course of one month. However, this approach would not typically be suitable for a long-duration mission, as the deviation grows in a secular manner.

Ramanan and Adimurthy [10] also studied lunar mapping orbits; however, they chose to abandon the search for a sun-synchronous orbit and instead focused on searching for a near-polar, circular, low-altitude lunar orbit with a long lifetime. For a circular 100-km-alt orbit, they found that the orbit lifetime depends directly on the inclination, minimizing at 20 days for an initial inclination of 11 deg and maximizing at over 730 days for an initial inclination of 95 deg.

Low-Thrust Stationkeeping

Some of the first works on low-thrust stationkeeping were conducted by Edelbaum [11] and Hunziker [12]. In 1964, Edelbaum [11] investigated optimal orbit-raising, rendezvous, and station-keeping using low-thrust systems. By finding a closed-form analytic solution relating changes in orbital elements to Lagrangian multipliers that defined the control variables, Edelbaum's method allowed for the optimal correction of all six orbital elements of a general elliptical orbit. In 1970, Hunziker [12] developed a method for stationkeeping a nearly circular equatorial orbit for a 24 h Earth satellite. Hunziker's method involved combining variation of parameters with a Newton–Raphson method to create a bang–bang controller.

Burt [13] analyzed the low-thrust control of orbital elements with Lagrange's planetary equations. In his analysis, expressions were derived that showed how all of the orbital elements could be controlled independently using small continuous thrusts. Burt applied these expressions to the problem of controlling the semimajor axis and inclination to those values needed for an Earth sun-synchronous orbit and generated a method for calculating the optimal low-thrust exhaust velocity. Later, Pollard [14] used control laws based on Burt's [13] approach to analyze a variety of missions, including transfers to geostationary Earth orbit and orbit disposal. The results from each mission were evaluated based on the required ΔV and the total trip time. Pollard [14] also analyzed the ΔV required to directly control the ascending node with an out-of-plane acceleration and showed that it was very costly in terms of propellant. He later stated that the preferred method for controlling the ascending node would be to make use of the J_2 effect and to control the altitude or inclination to achieve a desired ascending-node change. Note that because the analyses performed by Burt [13] and Pollard [14] were for Earth orbits, their approaches would not be valid for use on other bodies in space, such as the moon, which have complex gravity fields that cannot be approximated with analytic solutions. Many recent works on low-thrust stationkeeping also deal with Earth orbits, with a rising emphasis on the stationkeeping of geostationary orbits [15–17].

Obtaining Sun-Synchronous Orbits with Low-Thrust Systems

A number of studies have analyzed the process of generating and maintaining sun-synchronous orbits using low-thrust systems. However, as will be shown, a large majority of these works deal with sun-synchronous orbits about Earth, where the J_2 effect can be used to help obtain a solution.

One of the first works dealing with the low-thrust control of sun-synchronous orbits was performed by Barrett [18] in 1968. Barrett analyzed the problem of correcting injection errors for Earth sun-synchronous satellites. Because a sun-synchronous orbit exists for particular combinations of semimajor axis and inclination, an error in either of these two orbital elements will lead to a corresponding error in the rate of change of the ascending node. To eliminate the precession rate error, Barrett showed that there are three options: change either the semimajor axis or inclination so that the sun-synchronous condition is met or directly control the ascending node with an out-of-plane control acceleration. Each of these options was evaluated (based on total impulse) for correcting a 0.028 deg/day error in the precession rate. Of the three options, it was shown that directly controlling the ascending node is the most inefficient approach, with an excessive amount of required impulse, and controlling the semimajor axis was found to be the most efficient.

Later, Fosnight and Fosnight [19] developed an approach for controlling the nodal crossing time for sun-synchronous orbits using solar electric propulsion. The goal of this approach was to change from an initial sun-synchronous orbit at some initial ascending node to a sun-synchronous orbit at a *new* desired ascending node. To achieve the desired change in ascending node, the author used an approach of changing the orbit's inclination to induce a precession rate. The inclination change corresponded to a symmetric increase and decrease, such that at the end of the mission, the orbit would be sun-synchronous once again. The author showed that even with the inclusion of eclipses due to Earth's shadow, the desired amount of inclination change could be obtained using low-thrust levels.

Although the analyses performed by Barrett [18] and Fosnight and Fosnight [19] illuminate a variety of techniques for obtaining sun-synchronous orbits, their approaches are based solely on Earth orbiters for which the J_2 effect can be used to generate a majority of the required precession rate. In contrast, only one work [20] has been identified that addresses maintaining sun-synchronous orbit around other bodies in space. Leipold and Wagner [20] presented an approach to obtaining a forced sun-synchronous orbit about Mercury using solar sails. Because the J_2 term for Mercury is very small, the desired amount of ascending-node change must be performed entirely by control accelerations. Because of the high solar radiation pressure about Mercury, the authors find that a solar sail with a characteristic acceleration of 0.25 mm/s^2 is more than capable of producing the desired orbit rotation to maintain a sun-synchronous orbit. Both circular and elliptical orbits were studied, and it was found that eccentric orbits were more suitable for remote sensing. Finally, the authors also discuss how chemical and electric propulsion techniques could be used to obtain a Mercury sun-synchronous orbit. For a 300 kg spacecraft, the authors find that between 0.35 and 0.8 N of thrust would be required from electric thrusters to stationkeep this orbit.

In the perspective of the currently available work on low-thrust control of sun-synchronous orbits, the work presented in this paper makes important contributions in several areas. First, approaches are presented for generating sun-synchronous orbits about the moon, something that, to the authors' knowledge, has not been presented in the literature. Most important, this work presents an approach for stationkeeping about a body in space that has a complex gravity field. This requires a set of new techniques, because analytic solutions (which are often taken advantage of for Earth orbiters) are no longer as valid. Finally, by approaching the problem from a general nature, the methods developed in this paper could also be applied to missions at other locations.

Equations of Motion

In this section, the equations of motion used to model the motion of a low-altitude lunar orbiter are introduced. The equations incorporate perturbations from the Earth, sun, and nonspherical gravity field of the moon, which are the three primary perturbations that such a spacecraft would experience. Simulations are presented that show the long-term effects of these perturbations on the classical orbital elements.

Because it was desired to analyze the system dynamics in a reference frame fixed in the moon, a mean selenocentric reference frame [21] was chosen. A selenocentric frame is defined as a rotating reference frame with the origin at the center of the moon, where the $\hat{\mathbf{x}}$, $\hat{\mathbf{y}}$, and $\hat{\mathbf{z}}$ axes correspond to the moon's principal axes of inertia. In particular, the $\hat{\mathbf{x}}$ axis lies in the moon's equatorial plane directed toward Earth, the $\hat{\mathbf{z}}$ axis is directed through the moon's north pole, and the $\hat{\mathbf{y}}$ axis completes the right-handed coordinate system. The mean selenocentric reference frame differs from the true selenocentric reference frame in that it does not incorporate the physical librations of the moon. The effect of the librations will likely only cause small perturbations to the model and can be included in a future study.

Figure 1 shows the orientation of the four-body system that is considered in this work. Point O in Fig. 1 is an inertially fixed point in space from which the position vectors of the four bodies are defined. To compute the vectors $\boldsymbol{r}_{\odot\oplus}$ and $\boldsymbol{r}_{\oplus(}$, ephemeris-based equations are used. The $\boldsymbol{r}_{\odot\oplus}$ vector is found using ephemeris equations from the Jet Propulsion Laboratory's QUICK software [22,23], and the $\boldsymbol{r}_{\oplus(}$ vector is found from ephemeris equations given by Escobal [21]. Once these vectors are found, and noting that

$$\boldsymbol{r}_{(s/c} = x\hat{\mathbf{x}} + y\hat{\mathbf{y}} + z\hat{\mathbf{z}} \tag{1}$$

the other position vectors can be found (using Fig. 1) as

$$\boldsymbol{r}_{\oplus sc} = \boldsymbol{r}_{\oplus} + \boldsymbol{r}_{(s/c} \tag{2}$$

$$\boldsymbol{r}_{\odot sc} = -\boldsymbol{r}_{\oplus\odot} + \boldsymbol{r}_{\oplus(} + \boldsymbol{r}_{(sc} \tag{3}$$

$$\boldsymbol{r}_{\odot(} = -\boldsymbol{r}_{\oplus\odot} + \boldsymbol{r}_{\oplus(} \tag{4}$$

To obtain equations of motion that can be readily propagated using a numerical integrator, a state-space formulation was used to convert the system into a set of six first-order differential equations in terms of a state vector:

$$\mathbf{x}^T = [\,x_1 \quad x_2 \quad x_3 \quad x_4 \quad x_5 \quad x_6\,]^T \triangleq [\,x \quad y \quad z \quad \dot{x} \quad \dot{y} \quad \dot{z}\,]^T$$

where x, y, and z and $\dot{x}$, $\dot{y}$, and $\dot{z}$ correspond to the Cartesian position and velocity components of the spacecraft in the selenocentric frame. The six first-order differential equations of motion for this system are then

$$\dot{x}_1 = x_4 \tag{5a}$$

$$\dot{x}_2 = x_5 \tag{5b}$$

$$\dot{x}_3 = x_6 \tag{5c}$$

$$\dot{x}_4 = 2\omega_m x_5 + \omega_m^2 x_1 - \frac{\mu_\oplus r_{\oplus sc_x}}{|\boldsymbol{r}_{\oplus sc}|^3} - \frac{\mu_\odot r_{\odot sc_x}}{|\boldsymbol{r}_{\odot sc}|^3} + \frac{\mu_\oplus r_{\oplus(_x}}{|\boldsymbol{r}_{\odot(}|^3} + \frac{\mu_\odot r_{\odot(_x}}{|\boldsymbol{r}_{\odot(}|^3} + \nabla U_{(_x} + u_x \tag{5d}$$

$$\dot{x}_5 = -2\omega_m x_4 + \omega_m^2 x_2 - \frac{\mu_\oplus r_{\oplus sc_y}}{|\boldsymbol{r}_{\oplus sc}|^3} - \frac{\mu_\odot r_{\odot sc_y}}{|\boldsymbol{r}_{\odot sc}|^3} + \frac{\mu_\oplus r_{\oplus(_y}}{|\boldsymbol{r}_{\oplus(}|^3} + \frac{\mu_\odot r_{\odot(_y}}{|\boldsymbol{r}_{\odot(}|^3} + \nabla U_{(_y} + u_y \tag{5e}$$

$$\dot{x}_6 = -\frac{\mu_\oplus r_{\oplus sc_z}}{|\boldsymbol{r}_{\oplus sc}|^3} - \frac{\mu_\odot r_{\odot sc_z}}{|\boldsymbol{r}_{\odot sc}|^3} + \frac{\mu_\oplus r_{\oplus(_z}}{|\boldsymbol{r}_{\oplus(}|^3} + \frac{\mu_\odot r_{\odot(_z}}{|\boldsymbol{r}_{\odot(}|^3} + \nabla U_{(_z} + u_z \tag{5f}$$

In Eq. (5), μ is the gravitational parameter; ω_m is the rotational velocity of the selenocentric frame (2.66169×10^{-6} rad/s); u is the control acceleration; and the subscripts x, y, and z correspond to the Cartesian component of the particular vector.

The $\nabla U_{(}$ terms in Eqs. (5d–5f) are the components of the gradient of the lunar gravitational potential U and admit the perturbations due to the nonspherical lunar gravity model. A method for computing $\nabla U_{(}$ is given in [24]. The computation of the gravitational potential function requires knowledge of the lunar gravity field in terms of $C_{l,m}$ and $S_{l,m}$ coefficients. These coefficients are typically computed from observing tracking data from missions that have been conducted about the desired central body and are compiled to form gravity models. Current lunar gravity models containing C and S coefficients have been determined from previous lunar missions. The lunar gravity model used in this work is the LP165P gravity model obtained from the NASA PDS Geosciences Node, which contains lunar C and S coefficients up to a degree l and order m of 165×165 [2]. However, sufficient accuracy is obtained using only a subset of the coefficients, and numerical tests showed that using coefficients up to degree and order 25×25 was adequate for the nature of this study.

The equations of motion (5) are integrated using the `ode113` integrator in MATLAB, which is a variable-order and step-size Adams–Bashforth–Moulton PECE solver. The inputs that the program requires are the initial orbital elements, the initial Julian date, and the degree and order of the lunar gravity model to be used. The integrator also allows the user to select the relative and absolute error tolerances for the integration, both of which were chosen as 1×10^{-14} for all simulations in this work.

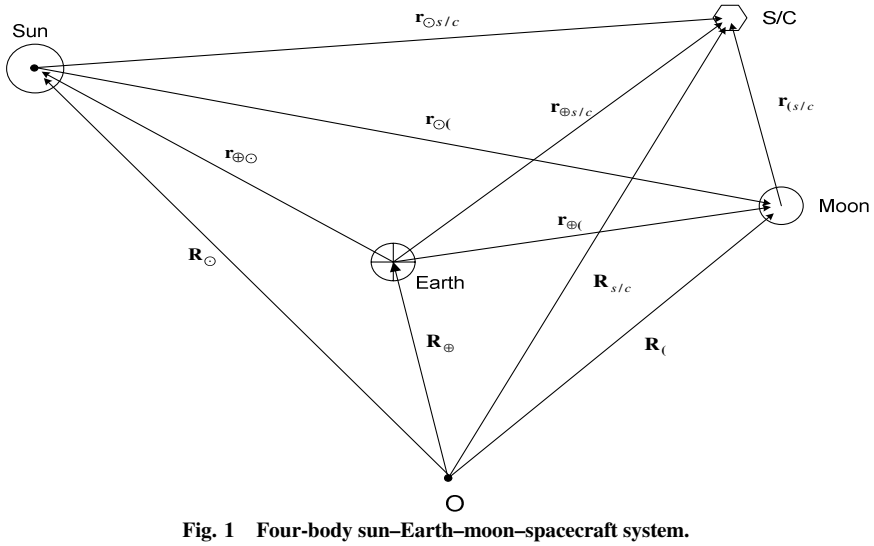

Fig. 1 Four-body sun–Earth–moon–spacecraft system.

Quasi-Frozen Orbit

It is well known [2,8,10,25] that perturbations of low-altitude lunar orbits are dominated primarily by the nonspherical lunar gravity field. The gravity field produces secular perturbations in the argument of periapsis and, in particular, the eccentricity. As a result, most low-altitude lunar orbits do not have very long lifetimes (typically less than 150 days for initial altitudes below 100 km). Because the objective of this work is to maintain a suitable mapping orbit for an extended period of time, a quasi-frozen orbit was chosen to slow the decrease in eccentricity to provide a longer orbit lifetime.

The term frozen orbit applies to any orbit in which the initial conditions have been chosen that result in one or more of the orbital elements remaining roughly constant (without the use of active control). For this work in particular, this amounts to selecting the initial eccentricity and argument of periapsis such that deviations in both parameters are small. Previous works [1,25] have shown that the argument of periapsis required to maintain a near-constant eccentricity must be either $\omega = 90$ or 270 deg. Through numerical simulations, it was found that a suitable initial eccentricity for minimizing argument-of-periapsis variations can be found as $e = 0.0337$. The combination of $e = 0.0337$ and $\omega = 270$ deg was thus chosen, which leads to a quasi-frozen orbit. The orbit is quasi-frozen because the eccentricity and argument of periapsis do not remain precisely constant, but are sufficiently bounded for purposes of this study.

Figure 2 depicts the results of a three-year (1089-day) simulation of the quasi-frozen orbit selected for this work. This simulation incorporated the perturbations due to gravity from the Earth and sun and due to the lunar gravity field up to degree and order 25×25. The initial orbital elements for the simulation are shown in Table 1. The initial orbit corresponds to a polar 60×185 km orbit.

It can be seen from Fig. 2 that over a three-year duration, none of the orbital elements change significantly from their initial values. Both the semimajor axis and inclination stay roughly constant, and the ascending node decreases by roughly 1.5 deg. Also, the eccentricity and argument-of-periapsis plots show that a quasi-frozen orbit is obtained in which both of the parameters are bounded. The eccentricity deviates from its initial value by roughly 0.05, and the argument-of-periapsis deviation is roughly 10 deg. Because the eccentricity and semimajor axis are both bounded, this implies that the periapsis altitude is also bounded and the orbit can be sustained for any desired length of time.

Table 1 Initial orbital elements for three-year simulation

Orbital parameter	Value
Semimajor axis a_i	1861 km
Eccentricity e_i	0.0337
Inclination i_i	90 deg
Ascending node Ω_i	45 deg
Argument of periapsis ω_i	270 deg
True anomaly ν_i	110 deg

Controller Design

The controller developed in this work was designed to meet three objectives:

1) Perform stationkeeping on the ascending node such that the sun-synchronous condition ($\dot{\Omega} = 0.9857\,\text{deg/day}$) is maintained within a desired error tolerance.

2) Perform stationkeeping on the inclination so that a polar orbit is maintained.

3) Satisfy both of the preceding objectives while minimizing the total amount of applied control acceleration.

The design selected for meeting these objectives involves alternating between regions of ascending-node control and inclination control. In particular, inclination control is performed over a specific latitude range across equatorial crossings, and ascending-node control is performed in the remaining regions between equatorial crossings. The remainder of this section details the development of this controller.

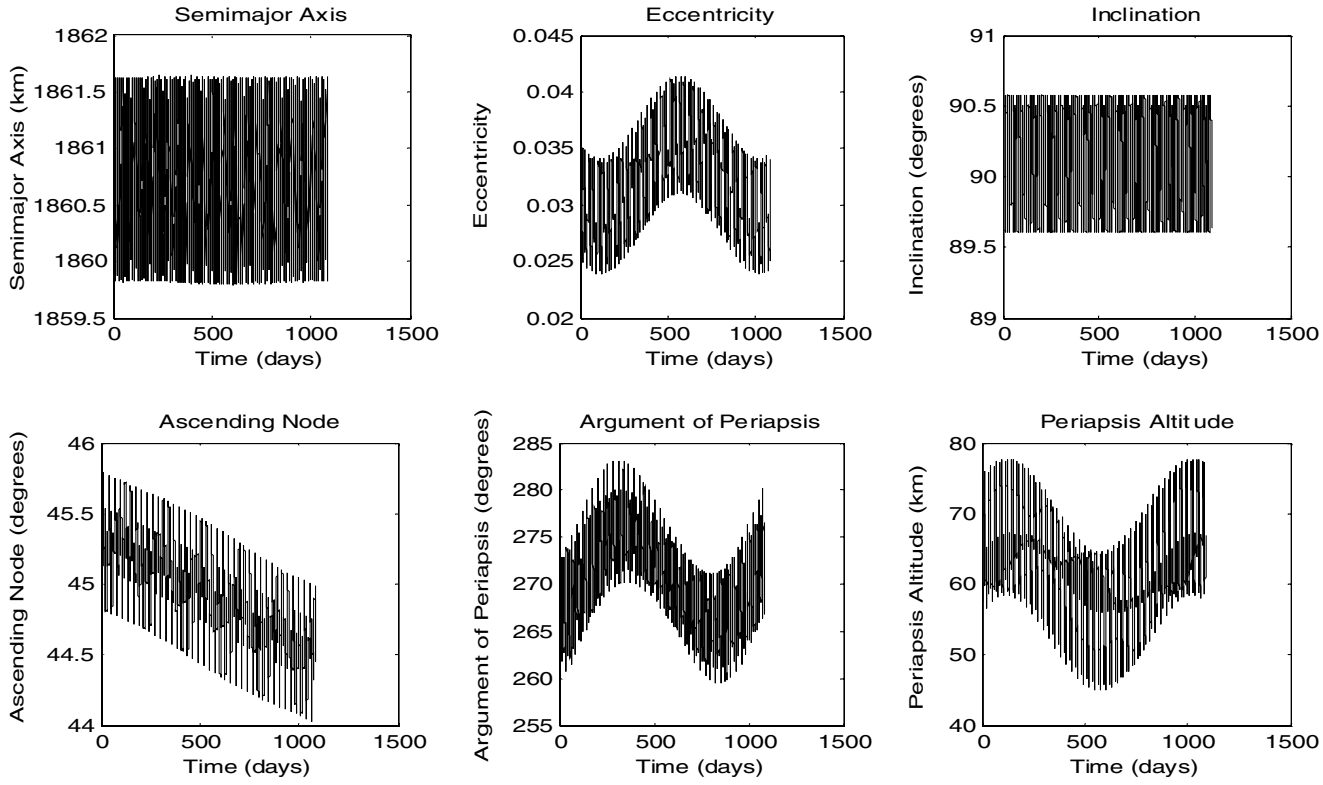

Fig. 2 Three-year propagation of quasi-frozen orbit.

Cost Function and Necessary Conditions for Optimality

The performance index is chosen with the form

$$J = \int_{t_0}^{t_f} L(\mathbf{x}, \mathbf{u}, t) \tag{6}$$

where t_0 and t_f are both known. No terminal constraints are imposed, and so the performance of this controller depends entirely on the selection of the cost function $L(\mathbf{x}, \mathbf{u}, t)$. This cost function is chosen as

$$L(\mathbf{x}, \mathbf{u}, t) = w_1 \cos^2 i_R(t) + w_2[\cos(\Omega_R(t)) - \cos(\Omega(t_0) + \dot{\Omega}_{\text{sunsynch}}(t - t_0) - \omega_m(t - t_0))]2 + w_3(u_x^2 + u_y^2 + u_z^2) \tag{7}$$

where $i_R(t)$ and $\Omega_R(t)$ are the actual (simulated) inclination and ascending node, respectively, taken with respect to the rotating frame; $\Omega(t_0)$ is the initial ascending node with respect to the inertial frame; and $\dot{\Omega}_{\text{sunsynch}}$ is the desired sun-synchronous rate (0.9856 deg/day). The first term in Eq. (7) indicates that it is desired to keep the inclination close to 90 deg, the second term indicates that it is desired to minimize the difference between the actual ascending node and the sun-synchronous ascending node, and the third term implies that the total control acceleration is to be minimized. Note that the inclination and ascending-node terms are expressed with cosine functions to simplify the partial derivatives of the cost function. Also, w_1, w_2, and w_3 are weighting parameters, used to define the priority of minimizing one element of the cost function over another. Setting either w_1 or w_2 to zero will indicate that control of the inclination or ascending node is not to be performed, allowing for the control of the respective element to be turned on or off. Finally, to provide consistent units in Eq. (7), w_1 and w_2 are unitless and w_3 is specified in units of s^4/km^2.

In terms of state-space coordinates, the cost function (7) can be written as

$$L(\mathbf{x}, \mathbf{u}, t) = w_1\left[\frac{(x_1x_5 - x_2x_4)^2}{(x_2x_6 - x_3x_5)^2 + (x_3x_4 - x_1x_6)^2 + (x_1x_5 - x_2x_4)^2}\right] + w_2\left[\frac{x_1x_6 - x_4x_3}{\sqrt{(x_2x_6 - x_3x_5)^2 + (x_4x_3 - x_6x_1)^2}} - \cos(\Omega(t_0) + \dot{\Omega}_{\text{sunsynch}}(t - t_0) - \omega_m(t - t_0))\right]^2 + w_3(u_x^2 + u_y^2 + u_z^2) \tag{8}$$

where, as before,

$$[x_1 \quad x_2 \quad x_3 \quad x_4 \quad x_5 \quad x_6]^T = [x \quad y \quad z \quad \dot{x} \quad \dot{y} \quad \dot{z}]^T$$

Now the necessary conditions of optimality [26,27] can be applied to find the optimal control history that minimizes Eq. (8). The first condition of optimality simply states that the system must follow the prescribed state dynamics, which are defined by Eq. (5) with the boundary condition $\mathbf{x}(t_0)$ given. The second condition specifies the costate dynamics as

$$\dot{\boldsymbol{\lambda}} = -\boldsymbol{\lambda}^T \frac{\partial \mathbf{f}(\mathbf{x}, \mathbf{u}, t)}{\partial \mathbf{x}} - \frac{\partial L(\mathbf{x}, \mathbf{u}, t)}{\partial \mathbf{x}} \tag{9}$$

It can be seen that solving Eq. (9) requires the calculation of

$$\frac{\partial \mathbf{f}(\mathbf{x}, \mathbf{u}, t)}{\partial \mathbf{x}}$$

(a 6×6 matrix) and

$$\frac{\partial L(\mathbf{x}, \mathbf{u}, t)}{\partial \mathbf{x}}$$

(a 6×1 column vector). Because of space considerations, these partials are not listed here, but it is noted that they are straightforward to obtain. Because there are no terminal constraints imposed, the boundary condition for the costate dynamics can be found to be

$$\boldsymbol{\lambda}^T(t_f) = \mathbf{0} \tag{10}$$

The final necessary condition is given by

$$\frac{\partial \mathbf{f}(\mathbf{x}, \mathbf{u}, t)^T}{\partial \mathbf{u}} \boldsymbol{\lambda} + \frac{\partial L(\mathbf{x}, \mathbf{u}, t)}{\partial \mathbf{u}} = \mathbf{0} \tag{11}$$

where, for this analysis,

$$\frac{\partial \mathbf{f}(\mathbf{x}, \mathbf{u}, t)}{\partial \mathbf{u}}$$

and

$$\frac{\partial L(\mathbf{x}, \mathbf{u}, t)}{\partial \mathbf{u}}$$

are obtained as

$$\frac{\partial \mathbf{f}(\mathbf{x}, \mathbf{u}, t)}{\partial \mathbf{u}} = \begin{bmatrix} 0 & 0 & 0 \\ 0 & 0 & 0 \\ 0 & 0 & 0 \\ 1 & 0 & 0 \\ 0 & 1 & 0 \\ 0 & 0 & 1 \end{bmatrix}$$

$$\frac{\partial L(\mathbf{x}, \mathbf{u}, t)}{\partial u} = [2w_3u_x \quad 2w_3u_y \quad 2w_3u_z] \tag{12}$$

Substituting Eq. (12) into Eq. (11) and solving for the control accelerations leads to

$$u_x = -\frac{1}{2w_3}\lambda_4 \tag{13a}$$

$$u_y = -\frac{1}{2w_3}\lambda_5 \tag{13b}$$

$$u_z = -\frac{1}{2w_3}\lambda_6 \tag{13c}$$

Equations (13a–13c) provide a useful relationship between the control accelerations and the costates, showing the simple relationship between the control accelerations and λ_4, λ_5, and λ_6.

This analysis results in 12 differential equations, Eqs. (5) and (9), with boundary conditions $\mathbf{x}(t_0)$ given and $\boldsymbol{\lambda}(t_f)$ specified by Eq. (10), for which the three control acceleration components are found via Eqs. (13a–13c). This two-point boundary-value problem is solved using an indirect shooting method [26,28] with an initial guess of $\boldsymbol{\lambda}(t_0) = \mathbf{0}$.

Implementation

Because of physical and geometric constraints, it is not possible to perform ascending-node control for an entire orbit. In particular, the ascending node cannot physically be controlled during equatorial crossings. Attempting to perform ascending-node control in these regions will lead to increasingly large control accelerations with ineffective control results. Also, it was found that it is not possible to perform ascending-node and inclination control simultaneously, as the control actions of maintaining the node and maintaining a polar orbit appear to counteract each other. For this reason, it was decided to alternate between regions of ascending-node-only and inclination-only control. More specifically, inclination control is performed in a latitude band $\pm\phi$ across equatorial crossings (with $w_2 = 0$), and ascending-node control is performed (with $w_1 = 0$) in the remaining regions over the northern and southern hemispheres.

In the regions of ascending-node control, special considerations must be made for the controller design outlined in the previous section. First, it is undesirable to terminate the controller in an

equatorial region. Comparing Eqs. (10) and (13), it is seen that constraining the final costates to zero also forces the final control accelerations to zero. This is obviously not beneficial near an equatorial crossing, as it is in these regions that the ascending node requires the largest control effort. On the other hand, during a polar crossing, the ascending node can be controlled with the least amount of control effort. It was therefore decided to terminate the controller at the polar crossing instead, with the resulting trajectory for ascending-node control regions composed of two segments. The first segment is a forward integration from the end of the equatorial region to the pole, and the second segment is a *backward* integration from the start of the next equatorial region back to the pole.

The proposed design implemented with the controller terminating at a pole crossing forces the control accelerations to zero at that point. Although it is a relatively good assumption that the ascending node will require minimal control effort at a polar crossing, realistically, a small but finite control acceleration will still be required when traversing a polar crossing. Thus, the controller would still attempt to force the control accelerations to zero when they should actually be finite, and it was found that this led to an excessive amount of control chattering with high initial control accelerations. A method for improving this behavior can be found through using an analytic solution and adjusting the desired final costates of Eq. (10). The analytic solution, which is described in a later section, allows for an approximation of the expected control accelerations over a polar crossing. Through the direct relationship between the control accelerations and the final three costates from Eqs. (13), the analytic solution also allows for an approximation of the final three costates. Thus, an estimate for the desired final costates can be found as

$$\boldsymbol{\lambda}^T(t_f) = [0 \;\; 0 \;\; 0 \;\; -2w_3 u_{\text{xanalytic}} \;\; -2w_3 u_{\text{yanalytic}} \;\; -2w_3 u_{\text{zanalytic}}]^T \quad (14)$$

Because no information is available to better estimate the first three costates, they are kept at zero. Although the condition of Eq. (14) is not necessarily optimal, what is important is that it leads to *better* results than would be seen if using Eq. (10) instead.

Also note that because ascending-node control is not performed over equatorial crossings, the ascending node would lag and increasingly deviate from the sun-synchronous condition if rotated at the rate of 0.9856 deg /day in the controlled regions. To compensate and remain close to the sun-synchronous condition, the ascending node is instead rotated at a rate that is slightly *higher* than 0.9856 deg /day. The required rotation rate depends on the latitude band $\pm\phi$ across the equatorial crossing, where no ascending-node control is performed. In this approach, the orbit plane is not precisely sun-synchronous, but averaged over an orbit, it remains sufficiently close for most mission requirements.

One final note must be made concerning the implementation of the preceding controller design. It was found that a singularity appears in the partial derivatives of Eq. (8) when the ascending node is either 0 or 180 deg. Thus, just like in the case of equatorial crossings, attempting to control the ascending node near either of these values leads to increasingly large control accelerations with ineffective control results. To address this complication, the controller is briefly switched to inclination control when the ascending node begins to enter one of these singularity regions.

Control Acceleration Dependence on ϕ

It was found that there is a very strong correlation between the latitude band $\pm\phi$, where no ascending-node control is performed, and the required control accelerations. In particular, increasing the latitude band decreases the amount of peak control applied to control the ascending node. However, this gain from lower control accelerations has an associated loss in terms of how precisely the ascending node follows the sun-synchronous line.

Figures 3 and 4 depict the control force magnitudes and ascending-node errors for one full orbit for two different values of ϕ: $\phi = 20$ and 40 deg. The first of these values, $\phi = 20$ deg, is the value that was selected for use in a one-year mapping simulation presented in a later section. In generating the control forces, a 1000 kg spacecraft mass was arbitrarily assumed. Also, the control weighting parameter w_3 was set to 8.0 s^4/km^2.

Figures 3 and 4 show the dependence of the control force magnitude and ascending-node error on the latitude band $\pm\phi$. Comparing Figs. 3 and 4, it is seen that by increasing the latitude band by 40 deg, the maximum control force magnitude required is decreased by roughly 0.2 N. Accompanying this loss is an increase in

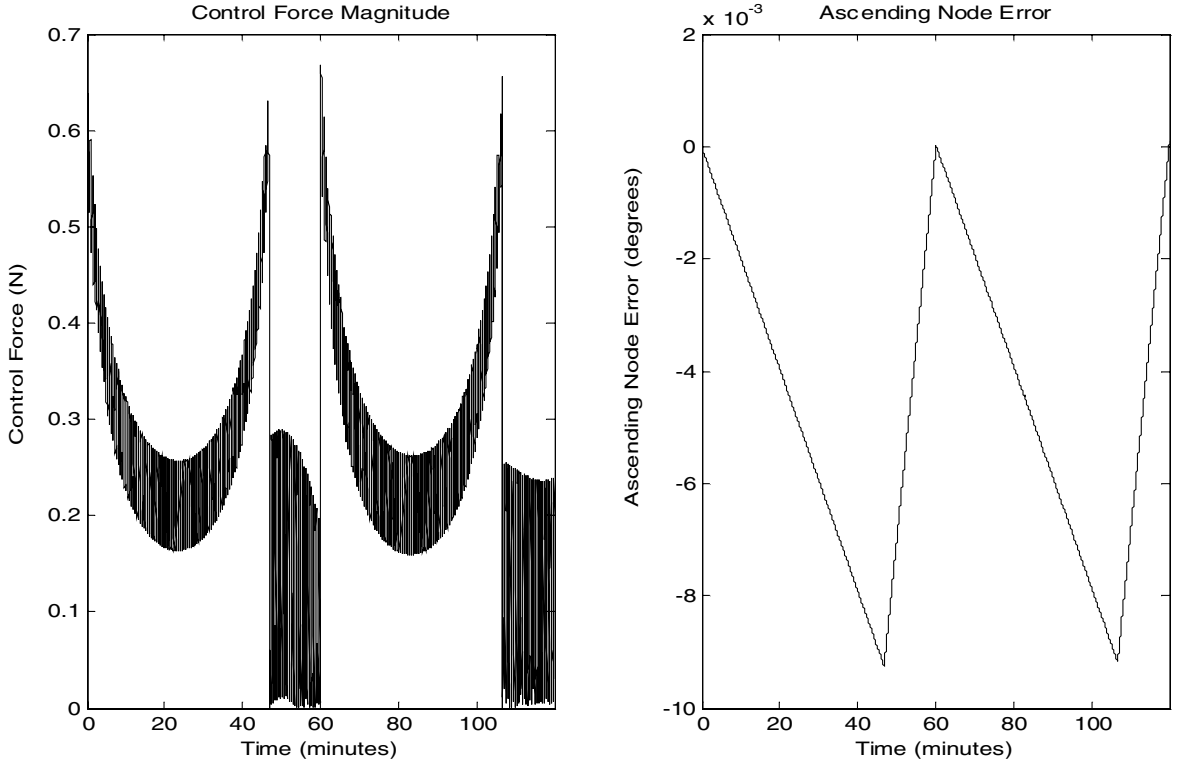

Fig. 3 Control force and ascending-node error for $\phi = 20$ deg.

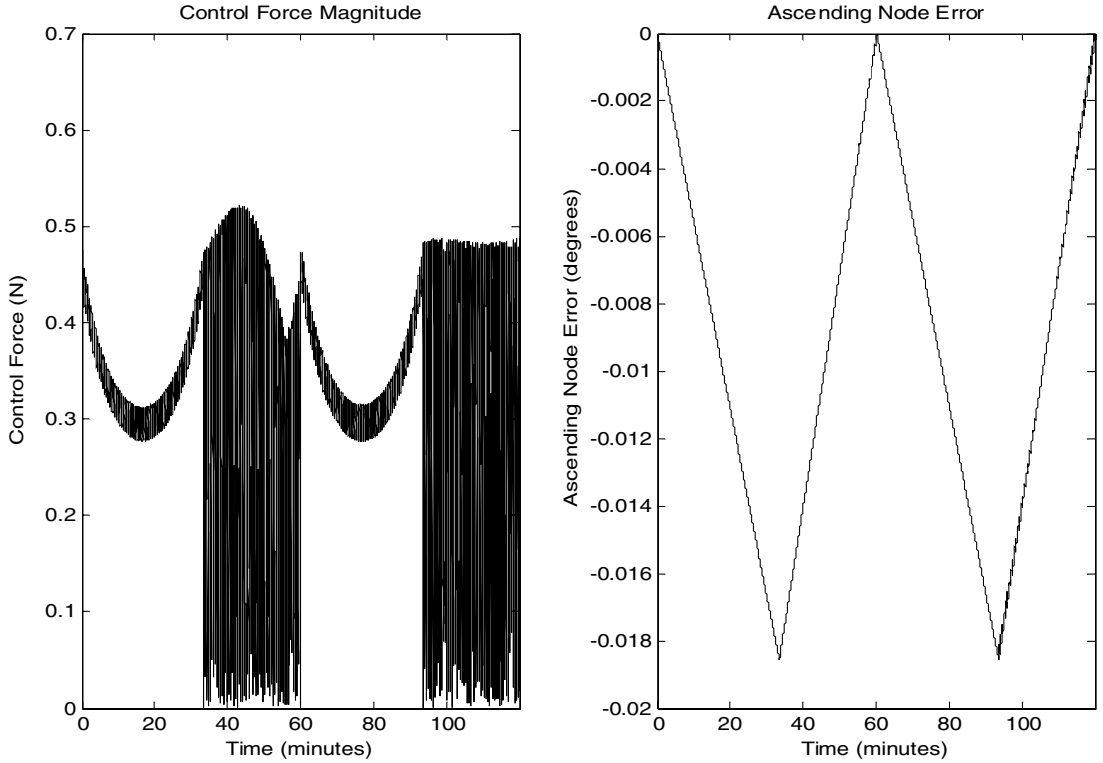

Fig. 4 Control force and ascending-node error for $\phi = 40$ deg.

the maximum ascending-node error from roughly 0.009 to 0.019 deg. This increase in the ascending-node error is unavoidable and occurs because a smaller percentage of the total orbit is spent toward controlling the ascending node. However, this analysis indicates that if the constraints on the sun-synchronous ascending are not as strict, it is possible to perform the mission with small control magnitudes.

Note from the control force histories in Figs. 3 and 4 that even after implementing the modified costate approach from Eq. (14) there is still a noticeable amount of chattering (particularly in the regions of inclination control). This type of control history can typically not be implemented, because modern control hardware cannot operate at the frequencies required to mimic the chattering effect. However, the control histories in Figs. 3 and 4 could feasibly be implemented if simple manipulations were performed. First, notice that in the regions of ascending-node control where chattering is present, the required force jumps between two control levels that are roughly equal in magnitude (maximum difference of 0.1 N from Fig. 3). Thus, a curve fit could easily be performed on the ascending-node control histories, yielding a history that could feasibly be implemented by control hardware while achieving similar performance on the chattering histories. Also, for the regions of inclination control, notice that the control histories involve jumping between a zero control force and a roughly constant force. If the maximum control forces in the inclination control regions were set constant at their average value, the control history could be implemented with an on–off thruster such as a pulse thruster. Because current pulse thrusters can perform pulses every second, it is expected that the on–off thrusting would yield very similar results to those produced by the chattering control history.

Analytic Solution

In this section, an approximate analytic solution for the sun-synchronous stationkeeping problem is found using Gauss's variational equations of motion [24]. This solution is presented for the simplified case of a spacecraft orbiting a perfectly spherical moon with no third-body effects. The analytic solution is then compared with the results from the controller described in the previous section for validation [and is used to adjust the final costates, as shown in Eq. (14)].

Gauss's variational equations of motion provide analytic equations for the rates of change of the classical orbital elements as a function of a perturbing acceleration:

$$\mathbf{F} = F_r\hat{\boldsymbol{r}} + F_\theta\hat{\boldsymbol{\theta}} + F_h\hat{\boldsymbol{h}}$$

In the $\hat{\boldsymbol{r}} - \hat{\boldsymbol{\theta}} - \hat{\boldsymbol{h}}$ frame, the $\hat{\boldsymbol{r}}$ unit vector is directed along the position vector of the satellite, the $\hat{\boldsymbol{h}}$ unit vector is directed normal to the orbit plane along the angular momentum vector, and the $\hat{\boldsymbol{\theta}}$ unit vector completes the right-handed coordinate system. In terms of the perturbing acceleration, the equation for the rate of change of the ascending node is given as

$$\dot{\Omega} = \frac{r\sin\theta}{h\sin i}F_h \tag{15}$$

where θ is the argument of latitude of the spacecraft and is calculated as the sum of the argument of periapsis and true anomaly. As expected, Eq. (15) shows that a change in the ascending node can only be caused by an acceleration F_h that is applied normal to the orbit plane.

Now, assume that no third-body forces are present and the perturbing acceleration $\mathbf{F}$ is provided from only applied control accelerations. By setting $\dot{\Omega}$ to the sun-synchronous rate (0.9856 deg/day), Eq. (15) can be rearranged to solve for a control force history that will produce a sun-synchronous orbit. This control force history can then be used to validate the control histories produced by the ascending-node controller from the previous section. Because the derivation of this analytic control history requires the assumption of a perfectly spherical moon with no third-body effects, for this comparison, the equations of motion (5) are simplified by setting $\mu_\oplus$ and $\mu_\odot$ to zero and by replacing $\nabla U_($ with

$$-\frac{\mu_(}{r_{s/c}^3}\boldsymbol{r}_{s/c}$$

By simplifying the dynamic model, it should be noted that the numerical control histories will be different from those shown in

Figs. 3 and 4, which were generated using all of the perturbations in Eq. (5).

Figure 5 shows a comparison of the analytic control history and the numerical control history obtained from the ascending-node controller with an assumed spacecraft mass of 1000 kg. The initial orbital elements for this simulation are shown in Table 1 with $\phi = 20$ deg.

Three plots are shown in Fig. 5: an analytic control history and two numerical control histories generated using the modified costate equation (14) and the unmodified costate equation (10). From an inspection of the two numerical histories, the usefulness of the modified costate approach is apparent. It is seen that not modifying the costates (and hence forcing the control accelerations to be zero at polar crossings) leads to both significant chattering and fairly large control force magnitudes. The modified costate approach decreases the chattering behavior and closely follows the same general pattern of the analytic solution with equivalent average control values. The primary difference between the analytic and modified numerical control histories is that a small amount of chattering remains in the numerical history. A possible explanation for this behavior is that the first three costates at the polar crossing are being constrained to be zero from Eq. (14). If estimates of what those costates should be during a polar crossing could be obtained, it is expected that the chattering effect would be further decreased and the two control histories would be much more similar.

Results

In this section, a one-year simulation is presented to show the effectiveness of the presented controller design in maintaining a polar sun-synchronous orbit. For this simulation, the weighting parameter w_3 is set to 8.0 s^4/km^2. For regions of ascending node or inclination control, the respective weighting parameters w_1 and w_2 are set to 1.0. The initial orbital elements for this simulation are shown in Table 1 and correspond to a low-altitude, near-circular, polar orbit. Figure 6 shows the orbital element histories for the simulation, and Fig. 7 shows the control force component magnitudes for a 1000 kg spacecraft.

As shown in Fig. 6, the ascending node rotates approximately 365.2 deg in 365.2 days as required. During the simulation, the ascending-node trajectory never varies from the desired sun-synchronous line by more than 0.1 deg. The inclination also remains near 90 deg, with a maximum deviation of approximately 0.025 deg. A polar sun-synchronous orbit has thus successfully been established and maintained. Also, it is seen that the quasi-frozen orbit from Fig. 2 is maintained despite the continuous thrusting that is being performed. This is to be expected, as out-of-plane thrusting has negligible effects on the in-plane orbital elements. The size of the orbit in Fig. 6 ranges from 77.94×167.27 km at $e = 0.024$ to 55.74×191.45 km at $e = 0.037$. Finally, although it appears from Fig. 6 that the periapsis altitude is approaching zero near the end of the mission, it would start increasing again according to Fig. 2 if the propagation continued.

Figure 7 shows that the polar sun-synchronous orbit is maintained using low-thrust levels. In particular, the maximum control force applied along the $\hat{\mathbf{x}}$ and $\hat{\mathbf{y}}$ directions is approximately 0.63 N. The control histories in the $\hat{\mathbf{x}}$ and $\hat{\mathbf{y}}$ directions indicate a beating phenomenon, which occurs due to the fact that the control forces will alternate in magnitude as the angular momentum vector is being rotated. It can also be seen that the control force in the $\hat{\mathbf{z}}$ direction is almost negligible. This is expected, because the inclination is close to 90 deg and the $\hat{\mathbf{z}}$ axis is thus almost entirely contained inside the orbit plane.

Assuming the average control force (0.5 N) is applied continuously for a year, a total ΔV of roughly 15 km/s would be required to maintain the polar sun-synchronous orbit for a year. For an ion thruster with an I_{sp} of 3000 s, this would amount to a total propellant mass of 416 kg. This is obviously a very large amount of propellant, but it gives an idea of what would be required to maintain a sun-synchronous orbit for a year. Although these results may imply that maintaining this orbit for a year would be difficult with current low-thrust technology, if the science requirements could be met by maintaining the orbit for a shorter duration, the required propellant mass can be drastically reduced. For example, because the moon will make one full rotation with respect to the orbit plane in roughly one month, it would be possible to globally map the moon with only a 1–2

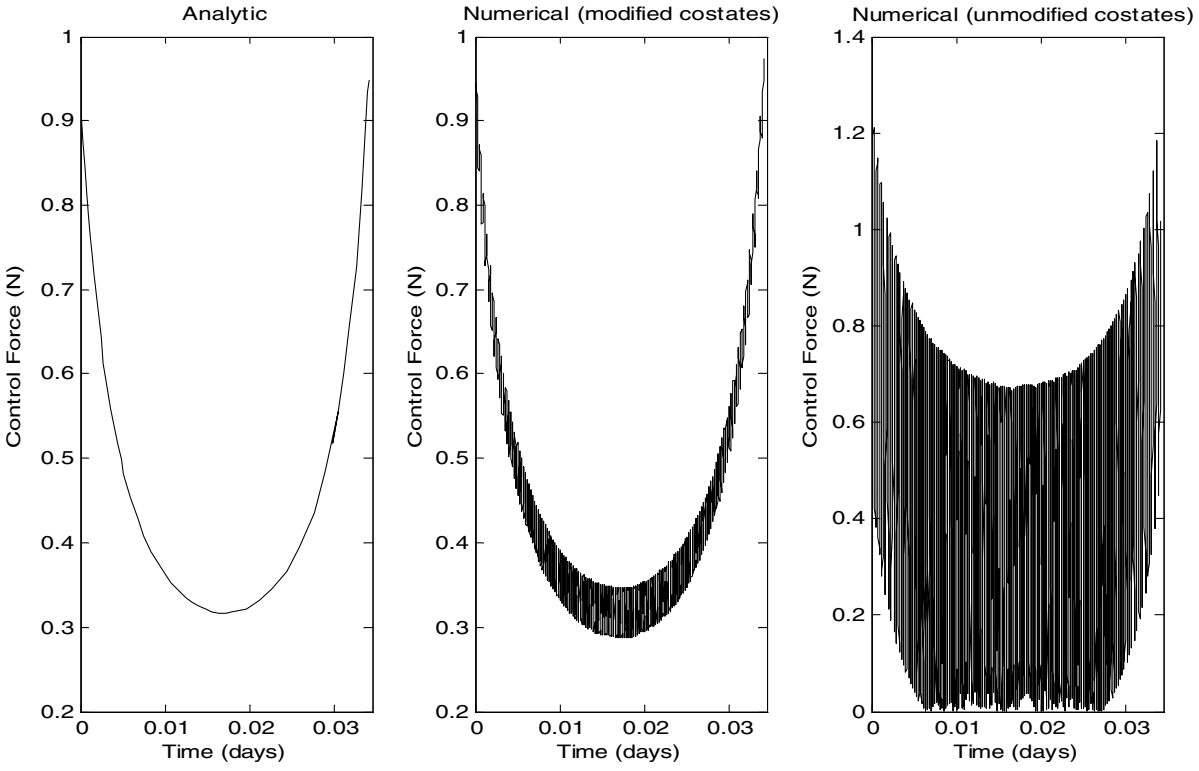

Fig. 5 Comparison of analytic and numerical control histories.

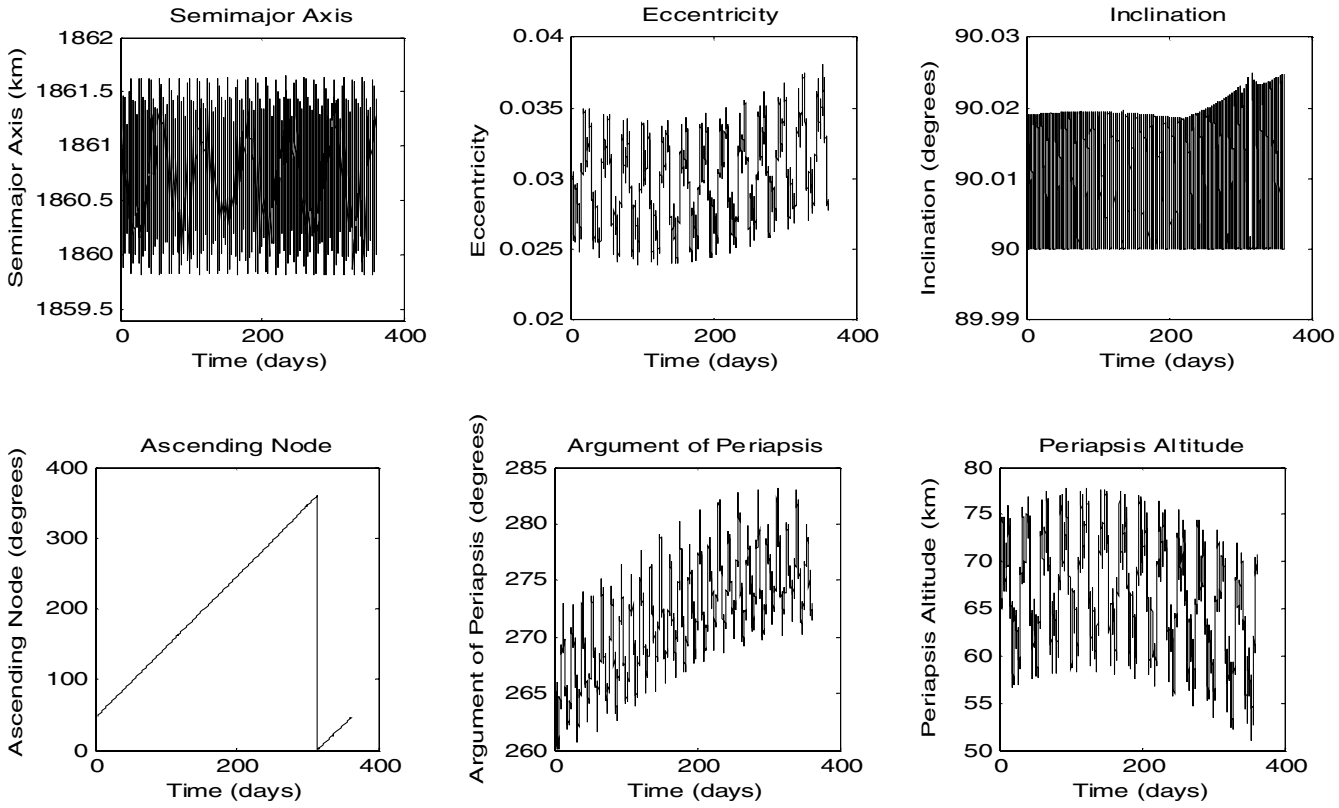

Fig. 6 Orbital element trajectories for one-year control simulation.

month mission. If the sun-synchronous orbit were maintained for one month, roughly 40 kg of propellant would be needed.

Note that although current continuous-thrust systems that have been flown in space may not necessarily be able to generate the thrust levels shown in Fig. 7, the levels *are* within the reach of many next-generation continuous-thrust systems. In particular, the thrust levels could feasibly be produced by a high-power arcjet thruster, and NASA is currently developing a Hall thruster (NASA-457M) that (although large) can generate thrust magnitudes ranging from 0.25 to 2.5 N [29]. However, implementing these types of thrusters would require next-generation power sources, such as high-efficiency solar cells or thermionic systems [30]. Another possible option would be

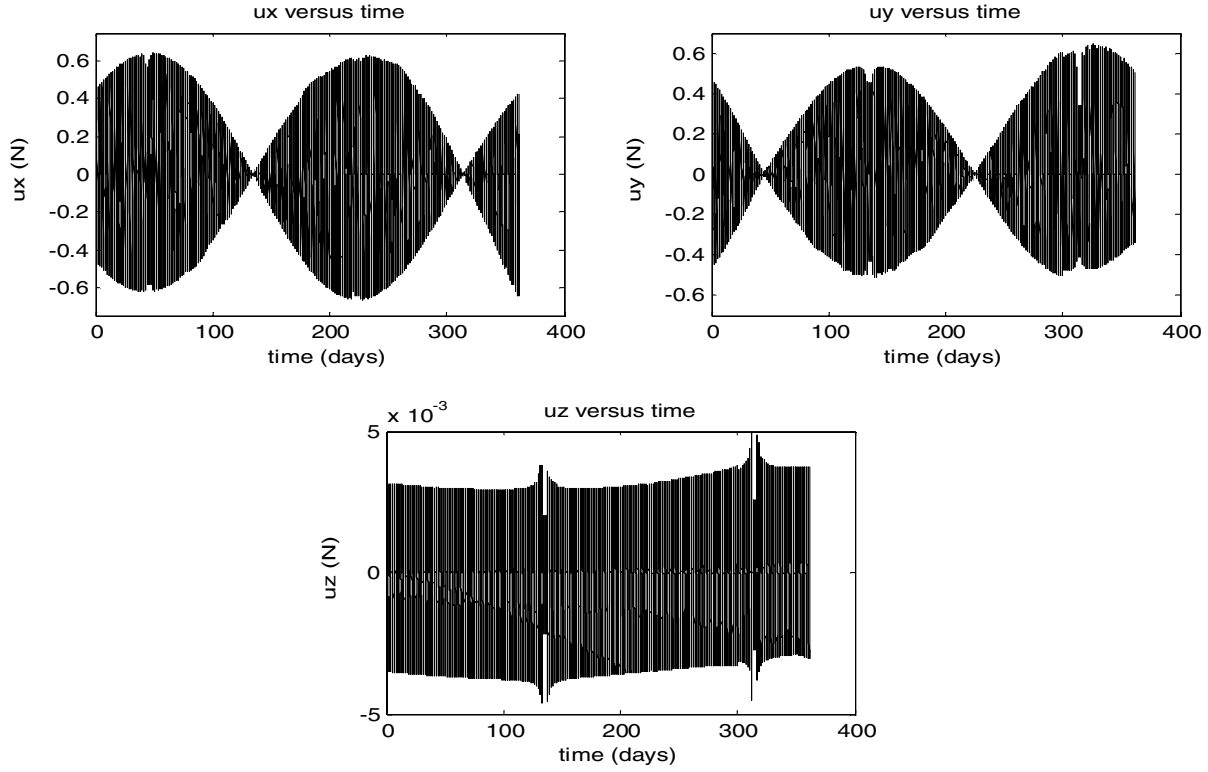

Fig. 7 Control force magnitudes for one-year control simulation.

to have three or more 200 mN ion thrusters onboard the spacecraft to provide the required thrust levels. Also note that if the mission could be completed with a 100 kg spacecraft, the thrust levels *would* be in the feasible range of current continuous-thrust systems, because the maximum force would only be roughly 63 mN.

Conclusions

A method for establishing and maintaining a polar sun-synchronous orbit using continuous-low-thrust systems has been presented. It is shown that by using optimal control theory, this orbit can be held for any desired length of time by alternating between regions of ascending node and inclination control. Also, it was found that by using an analytic solution to derive estimations for the desired final costates, a better solution is obtained than that from using the final costates prescribed by the optimal control theory analysis. Unfortunately, the resulting trajectories can only be considered suboptimal, but trajectories are still obtained that satisfy the required control objectives. A simulation of the method for a one-year mission was shown, and it was seen that the orbit can be maintained using thrust levels smaller than 0.7 N for a 1000-kg-class spacecraft.

The results from this paper show that a lunar sun-synchronous orbit can be somewhat expensive (in terms of propellant) to maintain, and so the mission designer would need to decide whether the improved science returns would outweigh the added propellant costs. Fortunately, there are possible alternatives to the one-year mission orbit studied in this work that would still be able to make use of a sun-synchronous orbit to globally map the moon. The first, and possibly most simple, alternative would be to only maintain the sun-synchronous orbit for a 1–2-month duration. That length of time would be sufficient to achieve global coverage and would require a smaller and more reasonable amount of propellant. Another possible alternative would be to perform the mapping mission at a higher altitude. Maintaining a sun-synchronous orbit at higher altitudes will require lower thrust levels, because the high altitudes will provide a larger moment arm for rotating the orbit plane.

Acknowledgments

This work was performed at the Missouri University of Science and Technology with support from a campus Chancellor's Fellowship and the NASA–Missouri Space Grant.

References

[1] Beckman, M. "Mission Design for the Lunar Reconnaissance Orbiter," 29th Annual AAS Guidance and Control Conference, Breckenridge, CO, American Astronautical Society Paper 07-057, Feb. 2006.

[2] Konopliv, A. S., "Recent Gravity Models as a Result of the Lunar Prospector Mission," *Icarus*, Vol. 150, No. 1, 2001, pp. 1–18. doi:10.1006/icar.2000.6573

[3] Hall, R. C., *Lunar Impact: A History of Project Ranger*, NASA, Rept. NASA SP-4210, 1977, Chap. 1.

[4] Day, D., *Surveyor—Lunar Exploration Program: The NASA Mission Reports*, Apogee Books, Burlington, ON, Canada, 2006, Chap. 1.

[5] Harvey, B., *Soviet and Russian Lunar Exploration*, Springer Praxis, New York, 2006, Chaps. 1–2.

[6] Regeon, P., and Chapman, R., "Clementine—Naval Research Laboratory Lunar Orbiter," 1994 Space Programs and Technologies Conference, AIAA Paper 1994-4590, 1994.

[7] Richon, K. V., and Newman, L. K., "Flight Dynamics Support for the Clementine Deep Space Program Science Experiment (DSPSE) Mission," *Advances in the Astronautical Sciences*, Vol. 90, No. 2, 1995, pp. 2045–2064.

[8] Folta, D., and Beckman, M., "The Lunar Prospector Mission: Results of Trajectory Design, Quasi-Frozen Orbits, Extended Mission Targeting, and Lunar Topography and Potential Models," *Advances in the Astronautical Sciences*, Vol. 103, No. 2, 1999, pp. 1505–1523.

[9] Park, S. Y., and Junkins, J. L., "Orbital Mission Analysis for a Lunar Mapping Satellite," *Journal of the Astronautical Sciences*, Vol. 43, No. 2, Apr.–June 1995, pp. 207–217.

[10] Ramanan, R. V., and Adimurthy, V., "An Analysis of Near-Circular Lunar Mapping Orbits," *Journal of Earth System Science*, Vol. 114, No. 6, Dec. 2005, pp. 619–626. doi:10.1007/BF02715946

[11] Edelbaum, T. N., "Optimal Low-Thrust Rendezvous and Station Keeping," *Journal of Spacecraft and Rockets*, Vol. 40, No. 6, 1964, pp. 1196–1201.

[12] Hunziker, R. R., "Low-Thrust Station Keeping Guidance for a 24-Hour Satellite," *AIAA Journal*, Vol. 8, No. 7, 1970, pp. 1186–1192. doi:10.2514/3.5870

[13] Burt, E. G., "On Space Manoeuvres with Constant Thrust," *Planetary and Space Science*, Vol. 15, No. 1, 1967, pp. 103–122. doi:10.1016/0032-0633(67)90070-0

[14] Pollard, J., "Evaluation of Low-Thrust Orbital Maneuvers," 34th Joint Propulsion Conference and Exhibit, AIAA Paper 98-3486, July 1998.

[15] Oleson, S. R., Myers, R. M., and Kluever, C. A., "Advanced Propulsion for Geostationary Orbit Insertion and North-South Station Keeping," *Journal of Spacecraft and Rockets*, Vol. 34, No. 1, 1997, pp. 22–28.

[16] Chan, J., Ariasti, A., and Hur-Diaz, S., "Comparisons of Two Station-Keeping Strategies for Ionic Propulsion Systems," *Proceedings of the Flight Mechanics Symposium*, NASA Goddard Space Flight Center, Greenbelt, MD, 28–30 Oct. 2003.

[17] Losa, D., "Electric Station Keeping of Geostationary Satellites: a Differential Inclusion Approach," *Proceedings of the 44th IEEE Conference on Decision and Control*, Inst. of Electrical and Electronics Engineers, Piscataway, NJ, Dec. 2005, pp. 7484–7489.

[18] Barrett, C., "Orbit Adjustment of Sun-Synchronous Satellites with Electric Propulsion," *Journal of Spacecraft and Rockets*, Vol. 5, No. 7, 1968, pp. 792–795. doi:10.2514/3.29359

[19] Fosnight, V. V., and Fosnight, R. M., "Nodal Crossing Changes for Sun-Synchronous Satellites with Solar Electric Propulsion," *Journal of Spacecraft and Rockets*, Vol. 21, No. 3, 1984, pp. 309–315. doi:10.2514/3.25654

[20] Leipold, M., and Wagner, O., "Mercury Sun-Synchronous Polar Orbits Using Solar Sail Propulsion," *Journal of Guidance, Control, and Dynamics*, Vol. 19, No. 6, 1996, pp. 1337–1341. doi:10.2514/3.21791

[21] Escobal, P. R., *Methods of Astrodynamics*, Wiley, New York, 1969, Chaps. 2–7.

[22] Skinner, D. L., "QUICK—An Interactive Software Environment for Engineering," *AIAA Computers in Aerospace Conference*, AIAA, Reston, VA, Oct. 1989, pp. 542–563; also AIAA Paper 1989-3051.

[23] Skinner, D. L., "Spacecraft Design Applications of QUICK," Aerospace Design Conference, Irvine, CA, AIAA Paper 1992-1111, Feb 3–6, 1992.

[24] Vallado, D. A., *Fundamentals of Astrodynamics and Applications*, 2nd ed., Microcosm Press, Torrance, CA, 2004, Chaps. 8 and 9.

[25] Folta, D., and Quinn, D., "Lunar Frozen Orbits," 2006 AIAA/AAS Astrodynamics Specialist Conference and Exhibit, Keystone, CO, AIAA Paper 2006-6749, 2006.

[26] Bryson, A., and HO, Y., *Applied Optimal Control*, Taylor and Francis, Philadelphia, 1975, Chaps. 2 and 7.

[27] Lewis, F., and Syrmos, V., *Optimal Control*, 2nd ed., Wiley Interscience, New York, 1995, Chap. 2.

[28] Betts, J. T. "Survey of Numerical Methods for Trajectory Optimization," *Journal of Guidance, Control, and Dynamics*, Vol. 21, No. 2, Mar.–Apr. 1998, pp. 193–207.

[29] Jacobson, D., and Manzella, D., "NASA's 2004 Hall Thruster Program," 40th AIAA/ASME/SAE/ASEE Joint Propulsion Conference and Exhibit, AIAA Paper 2004-3600, July 2004.

[30] Lanning, B., and Martin, D. "Survey of Current and Next Generation Space Power Technologies," 4th International Energy Conversion Engineering Conference and Exhibit, AIAA Paper 2006-4197, June 2006.